Nonlinear dynamics of slender inverted flags in axial flow

Mohammad Tavallaeinejad, Mathias Legrand, Michael Païdoussis

▶ To cite this version:

Nonlinear dynamics of slender inverted flags in axial flow

Mohammad Tavallaeinejad, Mathias Legrand, Michael P. Païdoussis
Mechanical Engineering Department, McGill University
Montreal, QC, H3A 2K6, Canada
mohammad.tavallaeinejad@mail.mcgill.ca,mathias.legrand@mcgill.ca

ABSTRACT

A nonlinear fluid-elastic continuum model of a slender cantilevered plate subjected to axial flow directed from the free end to the clamped one, also known as the inverted flag problem, is proposed. A nonlinear unsteady slender wing theory is employed to express the fluid-related forces acting on the plate. It is based on potential flow theory for inviscid fluids. The Euler-Bernoulli beam theory with exact kinematics and inextensibility is employed to derive the nonlinear partial integro-differential equation governing the dynamics of the plate. Discretization in space is carried out via a conventional Galerkin scheme using the linear modeshapes of the cantilevered beam. A Newton solver is implemented to obtain equilibrium solutions and integration in time is conducted using Gear's backward differentiation formula. A bifurcation diagram in terms of flow velocity is constructed in order to gain insight on the stability and post-critical behaviour of the system. It is shown that the undeflected static equilibrium is stable prior to a supercritical Hopf bifurcation giving rise to a flapping motion around the undeflected static equilibrium. By further increasing the flow velocity, the flag displays flapping motions around deflected static equilibria and change to fully-deflected static states at even higher flow velocities. These predictions are in excellent agreement with existing experimental data available in the literature.

NOMENCLATURE

H, L, h	Flag height/length/thickness
$Æ = H/L$	Flag aspect ratio
ρ, ρ_f	Flag/fluid mass density
D	Flag flexural rigidity
A	Flag cross-section area
I	Flag second moment of inertia
η	Material viscosity coefficient
c_d	External viscous damping coefficient
$t, x \in [0, L]$	Time and space parametrization
$u(x, t)$	Longitudinal in-plane deflection
$w(x, t)$	Transverse deflection
U	Free stream fluid flow velocity
$\alpha(x, t)$	Instantaneous angle of attack
$\theta(x, t)$	Angle of relative flow velocity
$\psi(x, t)$	Mid-plane slope = cross-section rotation
$T(t), V(t)$	Flag kinetic/potential energy
$\phi_r(x), q_r(t)$	rth modeshape/generalized coordinate
$F_\text{N}(x, t)$	Reactive component of fluid forces
$F_\text{R}(x, t)$	Resistive component of fluid forces
$V_n(x, t)$	Relative velocity normal to the centre-line
Π	Dimensionless flow velocity
$\bullet_t, [\bullet]_t, \dot{\bullet}$	First time derivative
$\bullet_x, [\bullet]_x$	First space derivative
$\bullet_{tt}, [\bullet]_{tt}, \ddot{\bullet}$	Second time derivative
$[\bullet]_{xx}, \bullet_{xx}$	Second space derivative

INTRODUCTION

An inverted flag is here understood as a cantilevered plate subjected to axial flow and clamped along its downstream edge in the flow. Applications, particularly in energy harvesting systems, have motivated recent studies in the literature. The flapping flag instability was first explored experimentally by Kim et al. [1] and later by Sader et al. [2] for various aspect ratios. Experimental observations have revealed that the flag aspect ratio can dramatically alter the dynamics. In particular, slender flags exhibit a buckling behaviour via a divergence instability. Wide flags, on the other hand, undergo a flapping motion prior to fully bending on one side via buckling. Moreover, the undeflected static equilibrium of inverted flags with smaller aspect ratios loses stability at higher critical flow velocities. These behaviours have been explored numerically in recent studies via three-dimensional computational simulations [3, 4]. In a remarkable work, Sader et al. [5] performed an experimental and theoretical investigation and provided an analytical framework to explore the stability and dynamics of inverted flags in the asymptotic limit of zero aspect ratio, employing a steady-flow model to represent the aerodynamic forces. They found the emergence of a bistable region wherein both the undeflected and the

1

deflected static regimes are stable, which cause inverted flag to display intermittent dynamics; any contribution of unsteadiness originating from the flow was neglected in their analytical model.

The present paper aims at deriving an analytical model accounting for flow *unsteadiness*. The resulting nonlinear dynamics is then investigated in the limit case of slender flexible plates. The sensitivity of the dynamics to the aspect ratio is also explored. The results are summarized in the form of bifurcation diagrams to identify the transition between various regimes.

MATHEMATICAL FORMULATION

In this section, the kinetic and potential energies of the cantilevered elastic beam shown in Fig. 1 are derived on the basis of the conventional nonlinear Euler-Bernoulli beam theory. Next, the virtual work associated with fluid-related forces is formulated. Finally, the equation of motion is obtained via Hamilton's principle.
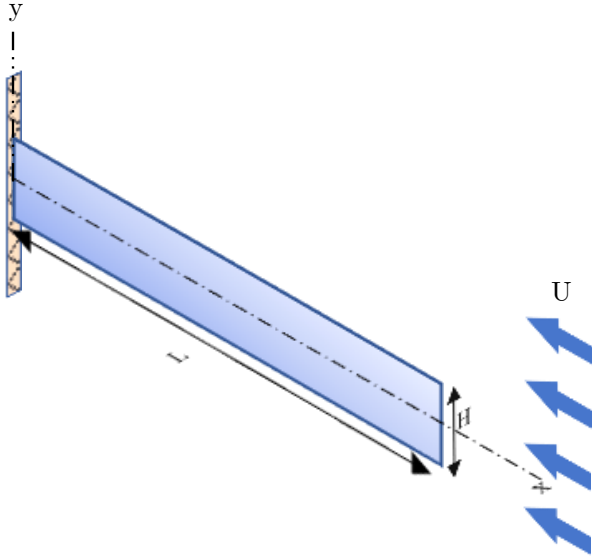

FIGURE 1: Inverted flag, idealized as a thin Euler-Bernoulli beam, in axial flow: free at the upstream and clamped at the downstream of the flow.

Potential and Kinetic Energies

Figure 2 shows a generic point at a distance z from the mid-plane on the cross-section of the flag; z and x stand for the transverse and axial directions, respectively, and t is time. Denoting by w the transverse motion, and by u, the longitudinal motion of the plate, the inextensibility assumption reads $(1 + u_x)^2 + w_x^2 = 1$. As a consequence,
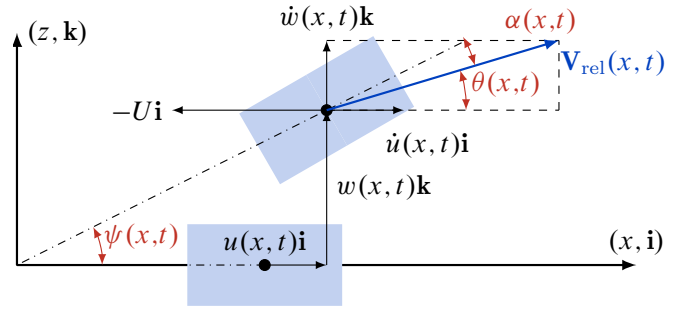

FIGURE 2: Generic infinitesimal element of the beam. The relative fluidbody velocity reads $\mathbf{V}_{\text{rel}} = (\dot{u}(x,t) + U)\mathbf{i} + \dot{w}(x,t)\mathbf{k}$.

w and u can be expressed in terms of the slope ψ, also the angle of rotation of the cross-section, and the velocities become

$$\dot{w}(x,t) = \int_0^x \dot{\psi}(s,t) \cos \psi(s,t) \, ds,$$
$$\dot{u}(x,t) = -\int_0^x \dot{\psi}(s,t) \sin \psi(s,t) \, ds. \tag{1}$$

The potential and kinetic energies are expressed as

$$T(t) = \frac{\rho A}{2} \int_0^L (\dot{w}^2 + \dot{u}^2) \, dx + \frac{\rho I}{2} \int_0^L \dot{\psi}^2 \, dx, \tag{2}$$

$$V(t) = \frac{D}{2} \int_0^L \psi_x^2 \, dx, \tag{3}$$

where $D = EHh^3/[12(1 - v^2)]$ and v denotes the Poisson's ratio.

Slender-body Nonlinear Model

The external aerodynamic force acting along the inverted flag can be decomposed into the reactive and the resistive forces, F_N and F_R, respectively. The resistive component models the viscous effects such as separation and drag, while the reactive force originates from the acceleration of fluid induced by the motion of the flag. The extension of large-amplitude elongated body theory [6,7] combined with large displacements (that is, large ψ) yields

$$F_N = \frac{\pi}{4} \rho_f H^2 \left(-\dot{V}_n + [V_n V_\tau]_x - \frac{1}{2} V_n^2 \psi_x \right), \tag{4}$$

where $V_n = -(\dot{u} + U) \sin \psi + \dot{w} \cos \psi$ and $V_\tau = (\dot{u} + U) \cos \psi + \dot{w} \sin \psi$ denote the normal and tangential components of the relative velocity of the element with respect to the incident flow, respectively. A closed form

of the resistive force can be obtained from semi-empirical expressions or analogical work based on potential-flow theory. In this paper, the resistive force is modelled on the basis of the Polhamus leading-edge suction analogy [8] in the form

$$F_R = \frac{\rho_f H U^2}{2}(K_p \sin\alpha \cos\alpha + K_v \sin^2\alpha), \quad (5)$$

with K_p and K_v being determined employing Bollay's nonlinear wing model [9]. As shown in Fig. 2, the instantaneous angle of attack can be expressed as $\alpha = \psi - \theta$ [10] where the relation $\tan\theta = \dot{w}/(U+\dot{u})$ holds. The virtual work done by the fluid-related forces normal to the plate is

$$\delta W_f = \int_0^L (F_N - F_R)(\delta w \cos\psi - \delta u \sin\psi)\mathrm{d}x. \quad (6)$$

Equation of Motion

Substituting Eqs. (2), (3) and (6) into the extended Hamilton's principle and using the following parameters: $x^* = x/L$, $t^* = t/\tau$, $\Pi = \rho_f SL^2U^2/D$, $\tau = L^2\sqrt{\rho A/D}$, $\mu = \rho_f L/(\rho h)$, $\beta = I/(AL^2)$, $k_a = \pi \mathcal{R}/4$, $k_p = K_p/2$, $k_v = K_v/2$, $c_d^* = c_d L^4/(D\tau)$, and $\eta_s = \eta/\tau$ generates the following nonlinear dimensionless equation of motion (with the asterisk notation dropped for brevity):

$$\beta\ddot{\psi} - \eta_s\dot{\psi}_{xx} - \psi_{xx} + \Pi\left(\cos\psi \int_1^x c_f(s,t)\cos\psi(s,t)\,\mathrm{d}s\right.$$

$$\left. + \sin\psi \int_1^x c_f(s,t)\sin\psi(s,t)\,\mathrm{d}s\right)$$

$$- c_d\left(\sin\psi\left[\int_x^1\int_0^s \cos\psi(\eta,t)\,\mathrm{d}\eta\mathrm{d}s\right]_t\right.$$

$$\left. + \cos\psi\left[\int_x^1\int_0^s \sin\psi(\eta,t)\,\mathrm{d}\eta\mathrm{d}s\right]_t\right)$$

$$- \sin\psi\left[\int_x^1\int_0^s \cos\psi(\eta,t)\,\mathrm{d}\eta\mathrm{d}s\right]_{tt}$$

$$+ \cos\psi\left[\int_x^1\int_0^s \sin\psi(\eta,t)\,\mathrm{d}\eta\mathrm{d}s\right]_{tt} = 0 \quad (7)$$

where

$$c_f = k_a\left[\frac{\mu}{\Pi}\left(\ddot{w}\cos\psi - \ddot{u}\sin\psi + 2\dot{\psi}(\dot{u}\cos\psi + \dot{w}\sin\psi)\right.\right.$$

$$+ \psi_x\left(\frac{1}{2}\dot{u}^2 - 3\dot{u}\dot{w}\cos\psi\sin\psi + \frac{3}{2}(\dot{w}^2 - \dot{u}^2)\cos^2\psi\right)$$

$$\left. - \dot{w}^2\right) + \sqrt{\frac{\mu}{\Pi}}\left(\psi_x(\dot{u} - 3\dot{u}\cos^2\psi - 3\dot{w}\sin\psi\cos\psi)\right.$$

$$\left. + 2\dot{\psi}\cos\psi\right) - \frac{1}{2}\psi_x(3\cos^2\psi - 1)\right]$$

$$+ k_p\sin\alpha_s\cos\alpha_s + k_v\sin\alpha_s|\sin\alpha_s|,$$

with $\alpha_s = \psi - \mathrm{atan}(\dot{w}/(\sqrt{\Pi/\mu} + \dot{u}))$. The clamped-free boundary conditions read $\psi(0,t) = 0$ and $\psi_x(L,t) = 0$. Equation (7) is discretized via a Galerkin expansion $\psi(x,t) = \sum_{r=1}^M \phi_r(x)q_r(t)$, where $\phi_r(x)$ denotes the rth eigenmode of the cantilevered beam and $q_r(t)$, its corresponding generalized coordinate. In this study, six modes are employed. This is sufficient to obtain converged results. The resultant set of nonlinear ordinary differential equations (ODEs) is solved using Gear's backward differentiation formula yielding the time histories of the amplitude of oscillation. Static equilibria $\psi_0(x)$ (together with $u_0(x)$ and $w_0(x)$) are retrieved via a nonlinear Newton procedure solving the time-independent discretized governing equations.

RESULTS AND DISCUSSION

The nonlinear dynamics of the system is now examined by means of bifurcation diagrams. Phase portraits and (flapping) flag shapes are also provided. The parameters used in the analysis are $L = 30\,\mathrm{cm}$, $h = 1\,\mathrm{mm}$, $\rho = 1200\,\mathrm{kg\,m^{-3}}$, $\rho_f = 1.2\,\mathrm{kg\,m^{-3}}$, $D = 2454\,\mathrm{N\,cm^2}$ and $\eta = 0.008$. The damping coefficient c_d is replaced by $2\zeta\omega$, where ζ is the modal damping ratio and ω is the first dimensionless linear natural frequency. The modal damping ratio, ζ, is set to 0.05 for the results obtained in this section.

Two configurations are considered: $H = 3\,\mathrm{cm}$ and $H = 10.5\,\mathrm{cm}$ corresponding to $\mathcal{R} = 0.1$ and $\mathcal{R} = 0.35$, respectively. Figures 3 and 4 depict the bifurcation diagrams for inverted flags with $\mathcal{R} = 0.1$ and $\mathcal{R} = 0.35$, respectively, as a function of the dimensionless flow velocity Π. Bold and dashed lines represent stable and unstable branches of the solution, respectively.

As seen in Fig. 3, no flapping motion is observed for $\mathcal{R} = 0.1$. When the flow velocity is increased, the inverted flag deflects abruptly from its stable trivial equilibrium (no deformation) to a stable deflected equilibrium via a subcritical pitchfork bifurcation at $\Pi = 28.9$. Also, the inverted flag may undergo a sudden large-amplitude deformation at lower flow velocities due to the emergence of a stable deflected equilibrium initiating from a saddle-node bifurcation at $\Pi = 8.6$. This behaviour agrees with other existing analytical findings [10, 5].

Figure 4 shows the bifurcational behaviour of the second case, that is a larger aspect ratio $\mathcal{R} = 0.35$. Unlike the first case, the inverted flag undergoes a large-amplitude flapping motion via a supercritical Hopf bifurcation at $\Pi = 2.05$; the amplitude of flapping increases with flow velocity. Remarkably, increasing the flow velocity causes a transition from a flapping regime around the undeflected equilibria to a deformed-flapping regime which the oscillation is around deflected equilibria. The latter motion
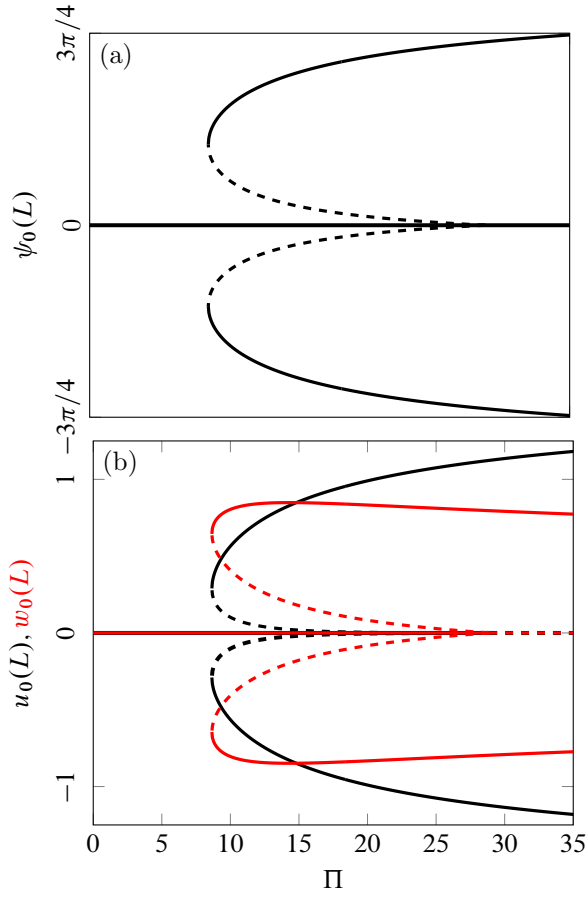
3

FIGURE 3: Bifurcation diagrams for $\mathcal{R} = 0.1$; (a) the tip slope and (b) the transverse/longitudinal displacement versus Π. Stable [——] and unstable [- - -] static equilibrium.
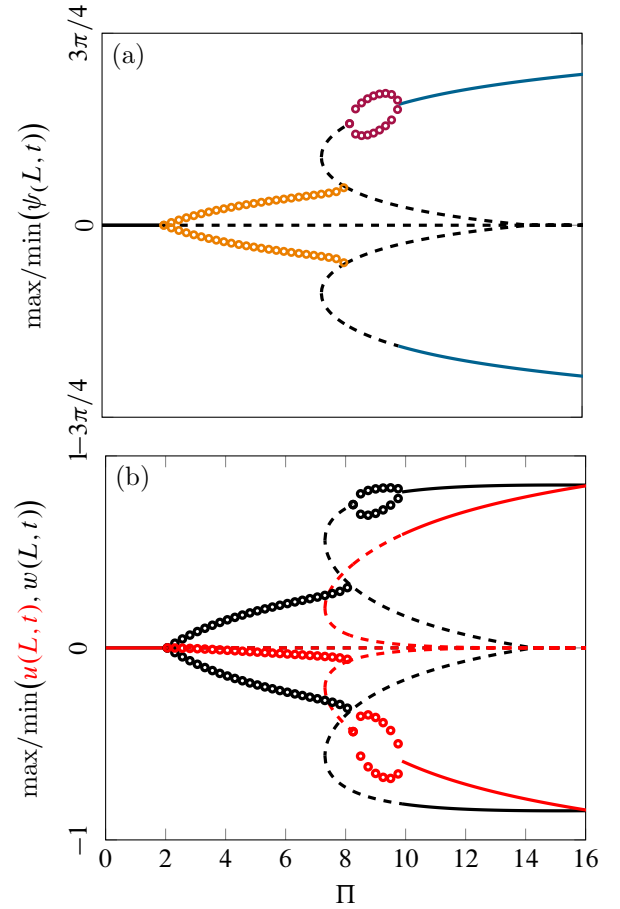

FIGURE 4: Bifurcation diagrams for $\mathcal{R} = 0.35$. (a) minimum/maximum values of the tip slope of the inverted flag. Stable static solution (undeflected stable equilibria) [——], unstable static solution [- - -], stable periodic solution (oscillation around undeflected equilibria) [○], stable periodic solution (oscillations around deflected equilibria) [○] and stable static solution (deflected static equilibria) [——]. (b) minimum/maximum values of the tip transverse/longitudinal motion. The colour scheme in (a) is used in Figs. 5 and 6.

dies out by further increasing the flow velocity. The inverted flag then undergoes a fully-defected regime via a secondary Hopf bifurcation at $\Pi = 9.95$. It should be noted that the response of the system is symmetrical with respect to the horizontal axis and the inverted flag may flap around deflected equilibria (buckled position) on either side. Flapping around one side is plotted *only*, so as to properly distinguish flapping around the undeflected static equilibria and flapping around the deflected equilibria.

Moreover, the fixed points of Eq. (7) are drawn as continuous (stable) and dashed (unstable) lines displaying a subcrtitical pitchfork bifurcation. This signifies that in case of introducing additional damping to the system, by touching the inverted flag using an external pole for instance [2], the static deflected solution turns into a stable equilibrium. As such, the inverted flag resides at this new induced equilibrium. This result is in line with the experimental treatment of Sader et al. [2]. From a comparison of the dynamics for $\mathcal{R} = 0.1$ and for $\mathcal{R} = 0.35$, it can be concluded that reducing the aspect ratio decreases the contribution of the reactive force, thus causing the divergence instability to take place at high flow veloci-

ties. For sufficiently large aspect ratios, on the other hand, the effect of the reactive component of the force becomes dominant and the inverted flag loses stability via a Hopf bifurcation leading to a periodic limit cycle. These findings are in excellent qualitative agreement with experimental observations reported in the literature.

Phase portraits are shown in Fig. 5 demonstrating the static equilibrium at $\Pi = 2.0$, the periodic limit cycle around undeflected static equilibrium at $\Pi = 8.0$, the periodic limit cycle around a buckled position at $\Pi = 9.5$, and finally, the static equilibrium at $\Pi = 20.0$. Snapshots of the configurations corresponding to the foregoing flow velocities are plotted in Fig. 6.
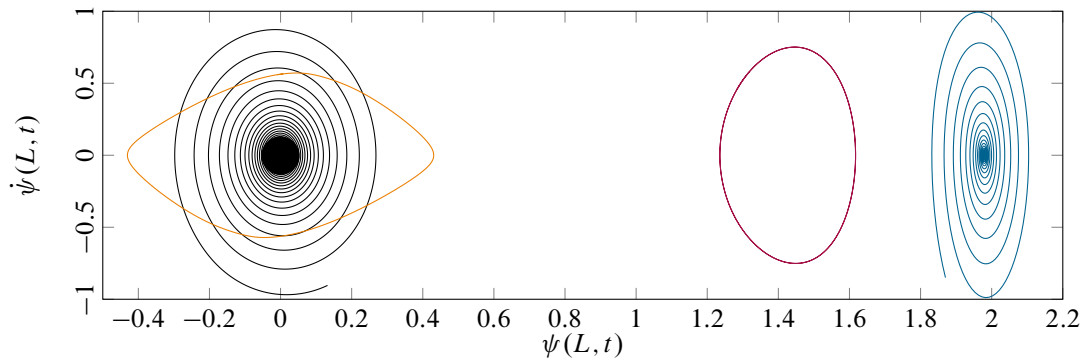
4

FIGURE 5: Phase portraits corresponding to Fig. 4. (a) $\Pi = 2.0$, (b) $\Pi = 8.0$, (c) $\Pi = 9.5$, (d) $\Pi = 20.0$.
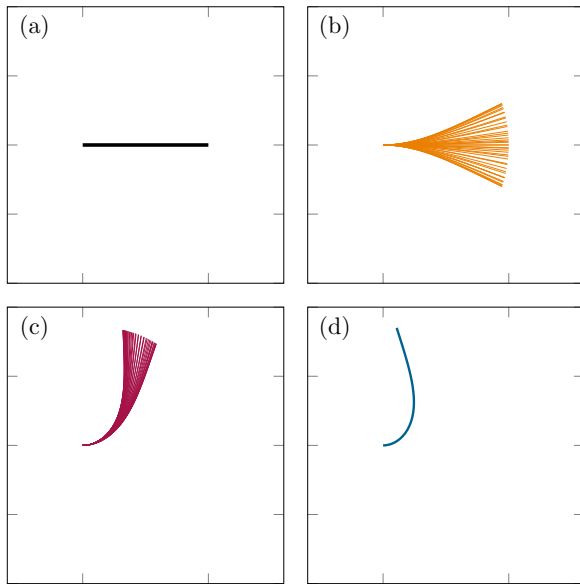

FIGURE 6: Flag motions in xz-plane corresponding to Figs. 4 and 5. (a) $\Pi = 2.0$, (b) $\Pi = 8.0$, (c) $\Pi = 9.5$, (d) $\Pi = 20.0$.

CONCLUSION

The nonlinear response of an inverted flag is investigated in this paper. An analytical model is developed taking into account the geometric nonlinearities and the flag's inertia. Fluid-related forces are treated independently employing the extension of large-amplitude elongated body theory. The nonlinear partial integro-differential equation is solved numerically using Gear's backward differentiation formula. Equilibrium solutions are obtained via implementing a nonlinear Newton solver. The results are presented as bifurcation diagrams, phase portraits, and flapping shapes to explore various static and flapping regimes.

The various responses indicate that the change in the flag's aspect ratio substantially alters the dynamics. Although inverted flags of small aspect ratio do not exhibit flapping motion for varying flow velocities, inverted flags of sufficiently large aspect ratios undergo a flapping motion. More specifically, flags of very small aspect ratio lose stability via a subcritical pitchfork bifurcation giving rise to the birth of multiple equilibrium states. In this case, any contribution of the unsteady terms of the flow can be neglected. In contrast, the time-dependent nature of the flow is expected to increase in strength with increasing aspect ratio. This results in considerably richer and more interesting bifurcational behaviour of the system. In particular, the inverted flag exhibits various dynamical regimes: (i) it first loses stability via a supercritical Hopf bifurcation in the first mode, the amplitude of which increases with flow; (ii) this transforms to a deformed-flapping motion; and (iii) finally, the system resides at the fully deflected state.

ACKNOWLEDGEMENTS

REFERENCES

[1] Kim, D., Cossé, J., Huertas Cerdeira, C., and Gharib, M., 2013. "Flapping dynamics of an inverted flag". *Journal of Fluid Mechanics,* **736**.

[2] Sader, J. E., Cossé, J., Kim, D., Fan, B., and Gharib, M., 2016. "Large-amplitude flapping of an inverted flag in a uniform steady flow–a vortex-induced vibration". *Journal of Fluid Mechanics,* **793**, pp. 524–555.

[3] Tang, C., Liu, N.-S., and Lu, X.-Y., 2015. "Dynamics of an inverted flexible plate in a uniform flow". *Physics of Fluids,* **27**(7).

[4] Gurugubelli, P. S., and Jaiman, R. K., 2017. On the mechanism of large amplitude flapping of inverted foil in a uniform flow. arXiv:1711.01065.

[5] Sader, J. E., Huertas-Cerdeira, C., and Gharib, M.,

2016. "Stability of slender inverted flags and rods in uniform steady flow". *Journal of Fluid Mechanics, 809*, pp. 873–894.

[6] Lighthill, M. J., 1971. "Large-amplitude elongated-body theory of fish locomotion". *Proceedings of the Royal Society of London. Series B, Biological Sciences, 179*(1055), pp. 125–138.

[7] Buchak, P., Eloy, C., and Reis, P. M., 2010. "The clapping book: Wind-driven oscillations in a stack of elastic sheets". *Physical Review Letters, 105*.

[8] Polhamus, E. C., 1966. "A concept of the vortex lift of sharp-edge delta wings based on a leading-edge-suction analogy". *NASA technical note*.

[9] Bollay, W., 1939. "A non-linear wing theory and its application to rectangular wings of small aspect ratio". *ZAMM-Journal of Applied Mathematics and Mechanics, 19*(1), pp. 21–35.

[10] Tavallaeinejad, M., Paidoussis, M. P., and Legrand, M., 2018. "Nonlinear response of inverted flags subjected to a steady flow". *Preprint*. [hal-01745147].